Cell cycle-dependent endocytosis of DNA-wrapped single-walled carbon nanotubes by neural progenitor cells

Swetha Chandrasekar,[1,2] Sophia Kuipa,[1] Ana I. Vargas,[1] Tetyana Ignatova,[3] Slava V. Rotkin,[4] and Sabrina S. Jedlicka[1,2,*]

[1]Department of Bioengineering, Lehigh University, Bethlehem, Pennsylvania; [2]Department of Materials Science and Engineering, Lehigh University, Bethlehem, Pennsylvania; [3]Joint School of Nanoscience and Nanoengineering, The University of North Carolina at Greensboro, Greensboro, North Carolina; and [4]Department of Engineering Science & Mechanics, Materials Research Institute, The Pennsylvania State University, Millennium Science Complex, University Park, Pennsylvania

ABSTRACT While exposure of C17.2 neural progenitor cells (NPCs) to nanomolar concentrations of carbon nanotubes (NTs) yields evidence of cellular substructure reorganization and alteration of cell division and differentiation, the mechanisms of NT entry are not understood. This study examines the entry modes of $(GT)_{20}$ DNA-wrapped single-walled carbon nanotubes (SWCNTs) into NPCs. Several endocytic mechanisms were examined for responsibility in nanomaterial uptake and connections to alterations in cell development via cell-cycle regulation. Chemical cell-cycle arrest agents were used to synchronize NPCs in early G_1, late G_1/S, and G_2/M phases at rates ($>80\%$) aligned with previously documented levels of synchrony for stem cells. Synchronization led to the highest reduction in SWCNT internalization during the G_1/S transition of the cell cycle. Concurrently, known inhibitors of endocytosis were used to gain control over established endocytic machineries (receptor-mediated endocytosis (RME), macropinocytosis (MP), and clathrin-independent endocytosis (CIE)), which resulted in a decrease in uptake of SWCNTs across the board in comparison with the control. The outcome implicated RME as the primary mechanism of uptake while suggesting that other endocytic mechanisms, though still fractionally responsible, are not central to SWCNT uptake and can be supplemented by RME when compromised. Thereby, endocytosis of nanomaterials was shown to have a dependency on cell-cycle progression in NPCs.

WHY IT MATTERS Every cell relies on the uptake or endocytosis of materials, such as proteins, cytokines, and even synthetic carbon nanomaterials, to perform its required cellular fate functions. Therefore, endocytosis is of interest for bringing therapeutic targets into cells. Recently, endocytosis has resurfaced as a topic of heavy debate, discussion, and discovery. Studying how materials get into the cell can aid in detangling trafficking to design higher-efficiency targeted drug- and gene-delivery therapies. Here we report the involvement of multiple endocytic pathways for bringing nanomaterials into neural stem cells and find a strong dependency of nanotube internalization on the cell cycle. This information can be harnessed to augment delivery of therapeutic materials based on the developmental stage of the cell.

INTRODUCTION

Carbon nanomaterial-based therapeutics have moved to the forefront of medicine in the last two decades, dominating applications such as controlled-release drug delivery, cell labeling, nanosensors, and scaffolds for tissue regeneration (1–6). The nanoscale size of

these materials and applicability of surface functionalization to assure biocompatibility of the nanotubes (NTs) make their transport across the blood-brain barrier (BBB) especially valuable, opening delivery access to the central nervous system. The unique optical and electronic properties of single-walled carbon nanotubes (SWCNTs) as well as their size range (1 nm diameter, ≥ 100 nm length) and mechanical strength, enable them to serve in a variety of applications involving crossing the BBB, from tumor targeting to gene therapy (4). While NTs have been shown to be instrumental in accessing areas previously thought of as difficult to

reach, other works have debated cytotoxicity and cellular damage related to size, purity, concentration, and functionalization (4,6−9).

As this was an early concern when developing experimental conditions, the material used in this work has been thoroughly characterized. The SWCNTs used in our studies are CoMoCat NTs wrapped with $(GT)_{20}$ single-stranded DNA oligomers (DNA-SWCNTs) (10,11). The DNA conjugation serves as a biomolecule mask to the cells, also substantially increasing nanomaterial solubility in aqueous buffer and inhibiting NT coalescence. Such a functionalization facilitates NT entry via endocytosis upon introduction in vitro (10,12) and preserves NT material dispersal in the form of individual tubes, as opposed to some earlier works (9,13−16). Biophysical characterization of the SWCNTs used can be found in our previous publications (17,18). Our previous studies in C17.2 neural progenitor cells (NPCs) allowed us to define the acceptable range of DNA-SWCNT concentrations (10 pM or lower) to be used for biological applications. Even in this range, there will be noticeable differences in cell morphology post DNA-SWCNT introduction (17). Over 16- to 72-h time periods post intracellular introduction of NTs, adherent cells have shown morphological alteration and diminished focal adhesion contact with the surface (19). Our studies have led to the conclusion that subnanomolar concentrations of well-dispersed nanomaterials, especially those that are DNA-wrapped, are in fact biocompatible.

Taking one step further, SWCNT introduction in the form of NTs dispersed in solution as a substrate or scaffold, have been shown to enhance rates of division and differentiation of stem cells (19−23). Our own studies have shown that differentiation of neural stem cells (NSCs) is augmented post incubation with SWCNTs (19). Therefore, it is postulated that the presence of the nanomaterials, in optimized concentrations and external conditions can upregulate aspects of natural cellular fate processes that can be harnessed to further understand the system, which can be used in the future to develop improved nanosensors and delivery therapeutics. Thus, a cellular- and molecular-scale analysis of the NT-cell system is required to comprehend the modification of cell developmental behavior in response to potential nanomaterial-based therapies as well as the downstream implications of cell-material interactions on these therapies.

A crucial step in determining the influence of NTs on NSCs was to prioritize the trafficking of materials through the cell, beginning with the method of entry. Nanomaterial entry mechanisms are not fully understood, and new studies have appeared recently detailing aspects of endocytic mechanisms and pathways that have eluded the field for decades (24,25). These entry mechanisms are accompanied by respective stimuli that trigger various downstream cellular responses and, accordingly, signal transduction changes in the cell. Unsurprisingly, this results in biochemical changes to the cell, vital to its growth and development, in addition to the cell's innate dynamic internal component reorganization.

While there are many aspects of neural stem processes that are yet to be understood, it is well known that the cell cycle lies at the crux of division, differentiation, and development of stem cells. Changes in cellular fate processes are generally linked to the cell cycle, the regulator of growth and development (26,27), and previous reports identify a link between endocytosis and cell cycle, defending the idea that cellular growth and development is interwoven with the trafficking of materials into and through the cell (28−33). Gaining control of the cell cycle via synchronization and maximizing single-phase yield are vital to resultant signal transduction pathways that lead to changes in downstream cellular fate processes. The overall mechanism of entry and the effect of specific phases of the cell on the endocytic mechanism will be key factors in deconvoluting the localization and correlation of SWCNTs among the subcellular organelles of NPCs.

Persisting speculation surrounding the entry, internalization, trafficking, and correlation of NTs within stem cells is a consequence, to some extent, of the lack of understanding of cell-cycle restructuring. As much as entry of NTs into the cell is a product of the cell cycle, the altered regulation of the cell cycle is also a by-product of the entrance of the NTs into the cell (34). Previously witnessed modifications in cell morphology, cytoskeletal organization, and differentiation could be tied to altered cell development. In the situation where growth, development, and differentiation are all in question, the cell cycle remains a critical underlying factor for the majority of the endocytic and developmental alterations observed. Therefore, studying how uptake translates further into downstream biochemical reactions is critical. Our study is focused primarily on the modes of entry of SWCNTs and how internalization changes based on the phase state of the cell.

MATERIALS AND METHODS

Cell culture

C17.2 mouse v-myc immortalized NSCs, a gift of Dr. Evan Snyder (Burnham Institute, La Jolla, CA), were cultured according to accepted protocol (35). NSCs were grown in Dulbecco's modified Eagle's medium (DMEM; Corning, Corning, NY) supplemented with 10% fetal bovine serum and 5% horse serum (Stasis Stem Cell Serum) at standard culture conditions of 37°C and 5% CO_2. 1× low potassium

Locke's buffer (10 mM HEPES, 5.6 mM KCl, 154 mM NaCl, 5.6 mM glucose, 1.2 mM MgCl$_2$, 2.3 mM CaCl$_2$, pH 7.4) was used for washing steps and all points where buffers are typically used.

Arrest and synchronization of cell cycle

Early G$_1$, late G$_1$/S, and G$_2$/M arrest was achieved through lovastatin (10 μM; AdipoGen, San Diego, CA), double thymidine (0.25 mM; Alfa Aesar, Ward Hill, MA) and nocodazole (400 nM; Sigma, St. Louis, MO) block, respectively. All agents were made up in DMEM (15% growth serum), and optimal concentrations and exposure times were determined to maximize percentage of cells in synchrony. Removal of chemicals and washing and replacement with medium or buffer was used to test release from arrest. NSCs were treated with arrest agents before being trypsinized and processed for flow cytometry. Cells were washed and fixed dropwise using 70% cold ethanol while vortexing, placed at 4°C for 30 min for complete fixation, and subsequently stained for DNA content using propidium iodide/RNase (BD Biosciences, Franklin Lakes, NJ). Flow cytometry was conducted using a BD FACSCanto hardware system and the BD FACSDiva software package. Gating of aggregates and doublets in the software resulted in high reliability of singlet cell data. FCS file analysis was conducted in both FCSalyzer and FlowJo. Data were fitted to a Watson-Pragmatic model where applicable.

"Leave-one-out" inhibition of endocytic mechanisms

Inhibition of endocytic mechanism receptor-mediated endocytosis (RME), macropinocytosis (MP), and clathrin-independent endocytosis (CIE) was effected by solutions of 0.45 M hypertonic sucrose (Fisher Chemical, Waltham, MA), 1 mM amiloride hydrochloride (Sigma-Aldrich, St. Louis, MO), and 1 μg/mL filipin complex (Sigma-Aldrich), respectively in 1× low K$^+$ Locke's buffer for 30 min of incubation at 37°C, knocking out one form of endocytosis and leaving the others undisturbed. Uninhibited control populations remained in 1× low K$^+$ Locke's buffer alone for 30 min. After inhibition the cultures were rinsed, leading into uptake testing with either SWCNTs or Tf-AF488.

Uptake assays and visualization

DNA-SWCNT uptake assay

NSCs seeded at low concentrations (3−5 × 10^3 cells/cm^2) on tissue-culture-treated borosilicate glass coverslips were allowed to grow for 48 h. Growth medium was removed from the cells, followed by a few gentle washes in Locke's buffer to remove any remnants of serum proteins. At this point, any synchronization/arrest (nocodazole, lovastatin, or thymidine) or endocytic inhibition (hypertonic sucrose, amiloride, or filipin) treatments were introduced. Cells were washed again with Locke's buffer post treatments. CoMoCAT SWCNTs wrapped with oligomeric (GT)$_{20}$ repeat DNA sequences were then suspended in sterile 1× low K$^+$ Locke's buffer at a low concentration of 5 ng/mL and incubated at 37°C for 8 h. After the incubation period the solution was aspirated, and the cells were washed in Locke's buffer to remove any uninternalized nanomaterials off the cell surface before being fixed in 4% paraformaldehyde. Coverslips were finally sealed onto slides with diamond antifade mountant prior to Raman imaging.

Hyperspectral imaging of SWCNTs in vitro

Raman hyperspectral imaging (532 nm excitation laser) was done on an Alpha300 R WITec confocal micro-Raman microscope (WITec, Ulm, Germany). Scans were taken at 50× and 100× magnification with a 0.1s integration time. Cell autofluorescence (2700−3015 cm^{-1}) and NT signature lines (310 cm^{-1}, 1590 cm^{-1}, 2630 cm^{-1}) were used to create spectral images, which were collected for a single set of 10 cells per sample. All 10 samples showed the same statistical distribution for SWCNTs in cells. Images were juxtaposed to show localization of internalized nanomaterials. 100× depth scans were taken starting from below the cell to above it, at intervals of $z = 0.1$ μm, to confirm NT residence. Visual (in a spectral map) and spectral (in single-point spectra) confirmation was used to collect internalization data.

Transferrin conjugate uptake assay

Cells grown to confluency were incubated with chemical synchronization agents for 24 h or endocytic inhibitory treatments for 30 min at 37°C. Cell monolayers were subsequently rinsed with warmed 1× low K$^+$ Locke's buffer and incubated with 20 μg/mL Transferrin-AlexaFluor 488 (Tf-AF488; Molecular Probes, Eugene, OR) in 1× Locke's buffer for 30 min at 37°C. Excess transferrin was rinsed off and cells were harvested, fixed with cold ethanol, and processed for flow cytometry. Uptake was discerned through relative fluorescence intensities read in the FITC channel of BD FACSCanto. Debris and aggregates were gated out to select for singlets, from which median fluorescence intensity was calculated from the resultant histogram peaks using FCSalyzer.

Viability assay

The LIVE/DEAD Viability/Cytotoxicity Kit (Invitrogen, Waltham, MA) was used to determine the average percentage of live cells in a population after each treatment. Live and dead cells were counted across three fields of view for three separate monolayers for each synchrony and endocytic inhibition treatment.

Statistical analysis

Where applicable, statistical analysis was determined by standard error measurements and post hoc analysis using Student's t-test. Significance levels were set at $p < 0.05$ (*) and $p < 0.01$ (**). Raman image scans were collected across two to three independent trials. All flow cytometry and cell assay data detailed throughout the study are presented as means of three or more independent experiments (across cell passages $n = 14$ to $n = 19$).

RESULTS AND DISCUSSION

Cell-cycle synchronization of embryonic neural stem cells

Many drugs and chemicals have been multipurposed for use in cell-cycle arrest and synchronization (36). While the range of reagents harnessed for this purpose is extensive, three methods of arrest were chosen for their ubiquity as well as their simplicity in mechanism of action. Agents with complex molecular mechanisms of action tend to affect multiple natural processes within the cell, resulting in higher rates of apoptotic response and permanent alterations. Therefore, molecular agents with evidence of direct effects on the actin cytoskeleton were avoided because of the vital role actin plays in conjunction with clathrin during RME. In an effort to maintain the natural state of the cell as
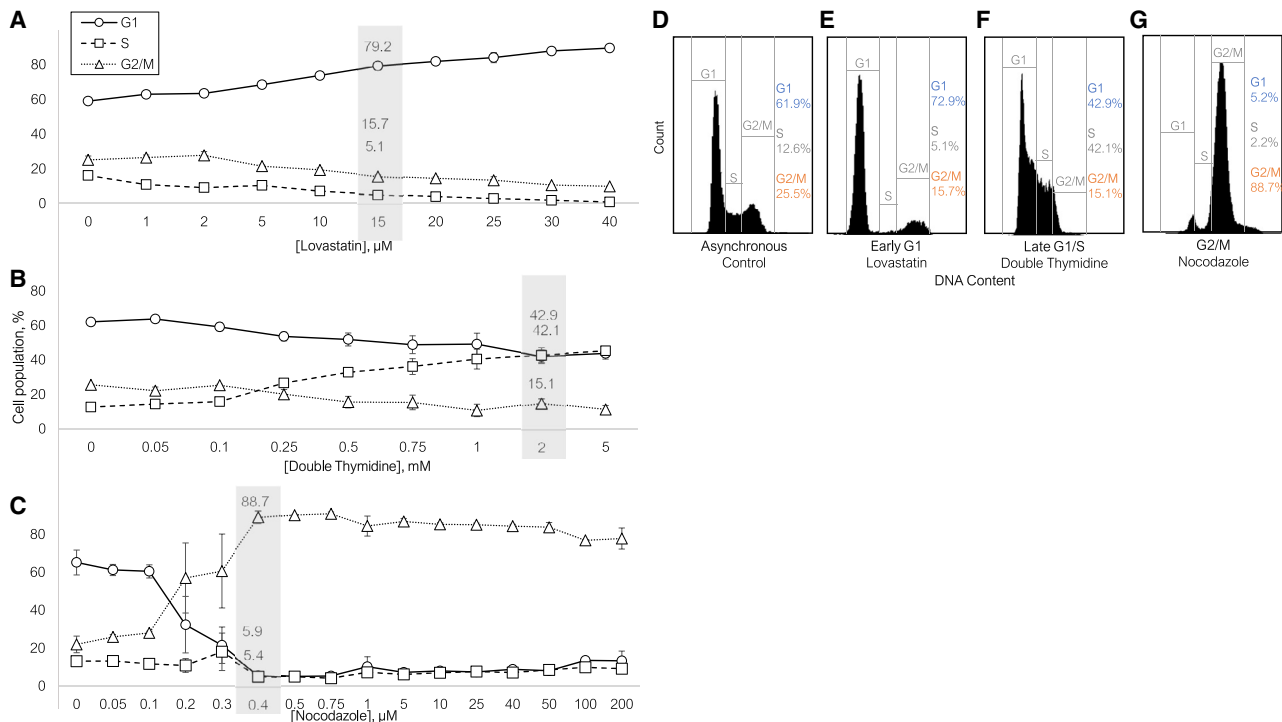
FIGURE 1 Optimization of chemical arrest of NSCs. Optimal achievement at the (A) early G$_1$ phase of ∼80% of NSC populations treated with >10 μM lovastatin (15 μM was chosen for the remainder of experiments), (B) G$_1$/S transition of ∼85% of NSCs by 2 mM double thymidine block, and (C) G$_2$/M transition of ∼89% of NSCs treated with the 400−750 nM range of nocodazole. 400 nM was chosen for the remainder of experiments to mitigate cell debris. Expectedly high variability of population distribution is visible at the onset of synchrony in the 200−300 nM range. For all treatments, concentrations were optimized to minimize chemical alteration of cells. Data were collected across three independent trials per concentration. Representative population distributions for chemically arrested NSCs. (D) asynchronous NSCs and average optimized synchrony over 24 h of 72.9%, 85%, and 88.7% of the cell population in (E) early G$_1$, (F) late G$_1$/S, and (G) G$_2$/M phases of the cell cycle, respectively as achieved through treatment by lovastatin (25 μM), double thymidine (0.25 mM), and nocodazole (400 nM). Cells were fixed and stained with propidium iodide (Becton Dickinson) for cellular DNA content and analyzed via flow cytometry. Singlet gating was applied to all data sets, and analysis was conducted using FCSalyzer.

best as possible, low concentrations of the pharmacological arrest agents lovastatin (early G$_1$), thymidine (late G$_1$/S), and nocodazole (G$_2$/M) were chosen.

Non-pharmacological methods of arrest, such as serum starvation and contact inhibition, have been used for decades to synchronize mammalian cells. However, it has been noted that serum deprivation while achieving synchrony simultaneously poises cells for a much higher rate of differentiation in embryonic stem cells (37). Chemical arrest agents can guarantee a more uniform synchrony. Its defined mechanisms of action ensure activity with molecular targets that do not interfere with the process of interest (36,38). While there are reports of differentiation caused by chemical-based synchrony of stem cells as well (39), our optimization showed that at ideal concentrations, increased apoptotic response and triggering of G$_0$ pathways are avoided while stimulating high arrest in the cell population (40). Simultaneously, our studies with serum starvation showed unequivocal differentiation of neural precursors into basal and apical neurons after 21 days (19). Single mechanism arrest followed by

release into subsequent phases yielded low rates of synchrony that were transient; hence, three different mechanisms were chosen to achieve sustainable synchrony.

Existing literature on the synchronization of primary cell lines (38,41,42), as well as stem cells (36) provides tested concentration ranges for the three drugs of interest and the percentages of synchrony they yield (43–46). These values from literature determined the upper and lower bounds of concentrations tested for each drug to find the highest synchrony possible for C17.2 NPCs. Nocodazole had the widest range of concentrations from nM to μM. While nM ranges led to lower rates of synchrony, μM concentrations were claimed to achieve higher synchrony but at the cost of permanently damaged microtubules. Thymidine was used fairly consistently in the lower mM range, while lovastatin was shown to work over a range of μM concentrations. Fig. 1, A−C details the optimization range for concentration-dependent synchrony by each treatment. Cells were treated with one of the three synchrony agents for 24 h for nocodazole and lovastatin,

or for 12 h in thymidine, 10 h in serum medium, and again 12 h in thymidine, to achieve a double thymidine block. The cells were then harvested and stained for cellular DNA content with propidium iodide to analyze via flow cytometry.

Fig. 1 A shows the results of the concentrations of lovastatin tested from 0 to 40 μM. While synchrony up to even 90% in early G_1 is achievable with lovastatin, a lower concentration accomplishing 80% synchrony was chosen to minimize damage and apoptotic cell density. With a double thymidine block, a consistent even split between late G_1 cells and S phase cells is evident, while G_2/M cells are at a normally functioning population size, showing that the cells are still proliferating and dividing. The nocodazole treatment (Fig. 1 C) shows that at 200 nM the crossover of G_2/M cells into the majority begins, but significant consistency is witnessed only above 400 nM. The flow cytometric histograms of DNA content shown in Fig. 1, E−G correspond to the final treatment concentrations chosen, as compared with the asynchronous population (Fig. 1 D). Ultimately, the optimization process revealed that 15 μM lovastatin, 2 mM thymidine, and 400 nM nocodazole led to the highest optimal synchronies of 80% early G_1, 85% G_1/S transition, and 89% G_2/M, respectively.

Additionally, it was important to rule out any adverse effects and chemical alterations caused by the arrest agents used. Table 1 shows the percentage viability of the cell populations after they were placed in each treatment for the times detailed in the methods below. This shows that all synchrony treatments had exceptionally high rates of viability, were comparable with the control, and remained unaffected by chemical alteration.

Cell-cycle dependency of DNA-SWCNT endocytic delivery

The synchronized cell populations were subsequently assessed for SWCNT uptake, the aim being to ascer-tain the influence of NT introduction on the cell-cycle arrested populations as compared with a control population. The results would also indicate whether NTs are accepted into the cell at varying levels depending on their phase, and ultimately whether this has any repercussions on how the cell processes the endocytosed material.

Previous studies support that the endocytic methods introducing certain materials into the cell vary based on the state of the cell (30,31,47−50). This implies that as the cell cycles through its natural phases, the corresponding primary method(s) of uptake oscillates accordingly. Inhibitory testing of all endocytic methods available for SWCNT entry shows how uptake varies according to the isolated individual mechanisms. A side-by-side comparison of SWCNT uptake based on cell cycle and methods of endocytosis will explain the process dependency and give a clearer understanding of how the mode of entry leads to localization and to downstream molecular changes as a result of their presence.

Fig. 2 shows the data detailing the SWCNT uptake and a summary of its dependence on phases of the cell cycle. Representative 50× hyperspectral scans of cells treated with each arrest agent are shown. The scans were collected by Raman spectroscopy, an established method of identifying carbon NTs in cells, as detailed previously (17,51−54). The SWCNTs in residence (blue boxes) are clearly distinguishable from the ones outside of the cell (white boxes). Several spectral signatures of NTs are recognized. We use mapping of the wavelengths for the radial breathing mode (near 300 cm^{-1}), G peak (1590 cm^{-1}), and G′ peak (2630 cm^{-1}). Cell autofluorescence should be differentiated from NT signal (C-H vibrations between 2700 and 3015 cm^{-1}). In some cases, spectral overlap with C-H vibrations will result in anomalies in the NT signature spectral maps (red boxes) to be eliminated. SWCNT residence was confirmed accordingly and, as needed, was investigated with depth profile scans under 100× magnification as shown with an example of an edge case in Fig. S1.

The experimental strategy developed for identifying NTs with Raman imaging is to begin with focusing on the bottom glass substrate and moving into the cell stepwise to focus on the bottom plane of the cell (where the spectral map is at its clearest or highest resolution). The height of the cell was then taken into account to move stepwise in the z direction up through the cell in order to characterize only internalized carbon NTs. Any NTs that were suspected to be surface-bound (marked with white boxes in Figs. 2, A−H and 3, A−H), were confirmed to be external and were not included in the uptake numbers (Figs. 2 I and 3 I). Only residence-confirmed cells (blue boxes) were included and plotted in Fig. 2 I.

TABLE 1 Reagents used for cell-cycle arrest and chemical endocytic inhibition, their target processes, and resultant cell viabilities after 30 min (endocytic inhibition) and 24 h (cell-cycle arrest) treatments on neural progenitor cells

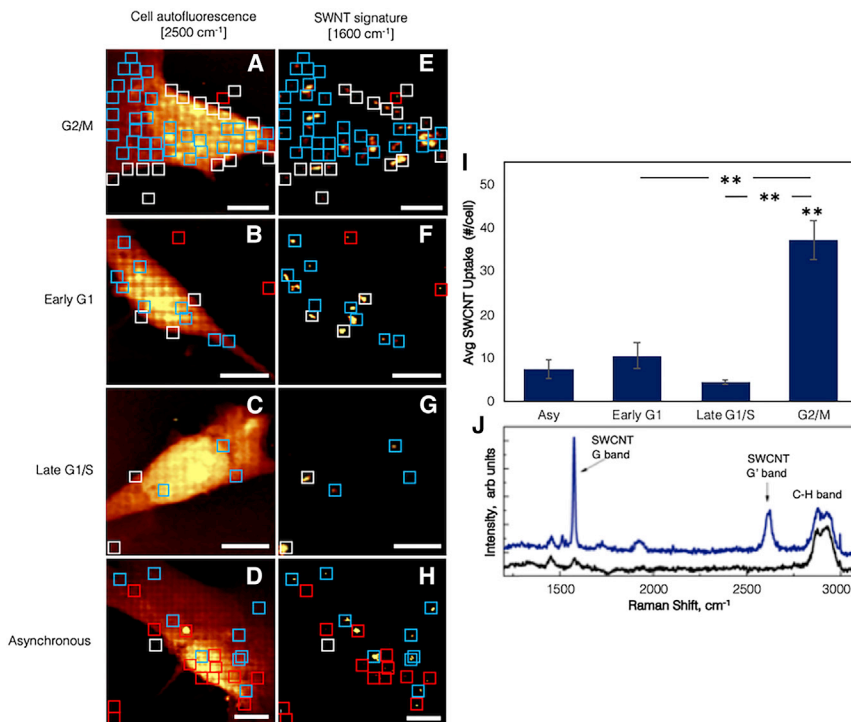| Process	Inhibitor	Inhibition/ arrest of	Cell viability (%)
Cell cycle	nocodazole	G_2/M	95.1 ± 1.1
	thymidine	late G_1/S	87.8 ± 1.1
	lovastatin	early G_1	98.8 ± 0.2
Endocytosis	hypertonic sucrose	receptor-mediated endocytosis (RME)	98.9 ± 0.2
	amiloride	macropinocytosis	95.8 ± 1.1
	filipin	clathrin-independent endocytosis (CIE)	98.8 ± 0.4
Control	low K^+ Locke's buffer		98.2 ± 0.2

FIGURE 2 Hyperspectral imaging of chemically arrested NSCs. Autofluorescence of (A−D) NSCs and (E−H) DNA-SWCNTs in NSCs arrested by (A, E) nocodazole in G_2/M, (B, F) lovastatin in early G_1, and (C, G) double thymidine in late G_1/S phases of the cell cycle, via confocal micro-Raman microscopy as compared with a (D, H) control, asynchronous cell. SWCNTs with intracellular residency (*blue boxes*) confirmed by 100× images taken at various points along the depth of the cell. Some SWCNTs remain adhered to the outer cell membrane (*white boxes*). Red boxes indicate innate C-H vibrations associated with cell autofluorescence, bubbles, or cosmic rays. (I) Average SWCNT uptake post cell cycle chemical synchronization. (J) Representative spectral signatures of an SWCNT (*top*) and autofluorescence of the cell (*bottom*). **p < 0.01. Scale bars, 10 μm.

This strategy also includes several procedures to mitigate the concern of aggregated nanomaterials. First, as previously explained in previous work (17), RBM modes can be used to discriminate the aggregates from individual NTs. The G and 2D modes also show characteristic broadening upon aggregation that can be resolved from data statistics. In the event that aggregation of NTs is detected, the instance would be included in the statistical count. However, the use of an extremely low concentration of NTs is an important distinction of this work from a number of previous ones, where the SWCNT concentration used was many orders of magnitude larger and aggregation happened permanently.

The data in Fig. 2 *I*, obtained by counting the average number of NTs per cell from hyperspectral images (Figs. 2, *A−H*), summarizes the findings and indicates a large increase in uptake for G_2/M arrested cells, as well as an insignificant increase in uptake in early G_1 cells, as compared with an asynchronous cell population. A reduction in uptake is noted in late G_1/S arrested cells.

Double thymidine block treatment resulting in majority G_1/S transition cells led to a 40% decrease in endocytic uptake, suggesting that the late G_1 and early S phases are selective to uptake of materials. Simultaneously, samples of primarily early G_1 and G_2/M cells led to 40% and 390% increases in uptake of SWCNTs, respectively. Existing studies contradictorily propose that clathrin-mediated endocytosis (CME) is either in-

hibited or unaffected during the G_2/M phase (30,31). Our data show that the G_2/M phase is an avid acceptor of materials, as it has a fourfold higher yield of internalized NTs per cell on average when compared with control cells. This proves the dependency of uptake on the mitotic phase of the cell cycle.

The disproportionately high uptake of SWCNTs during nocodazole arrested G_2/M cells suggests either one method of uptake is augmented during mitosis or that multiple pathways are contributing simultaneously to internalization. To unravel this further, CME and the importance of the vital protein clathrin during the mitotic phase is an important and well-studied place to start. Clathrin is involved in the generation of new vesicles as well as mitotic spindle stabilization (55). Along with an adapter protein, AP-2, the clathrin complex produces clathrin-coated vesicles (CCVs) to facilitate transport of materials across the cell (32). Reduced dynamics of clathrin will result in lower production of CCVs to carry forward typically observed rates of RME. Some reports suggest that clathrin is impaired during mitosis, reducing the activity of CME during mitosis (56), even stating that transferrin uptake is completely inhibited in mitotic cells despite the presence of transferrin receptor (TfR) at the cell surface to accept cargo (30). Overall, the sharp increase in uptake of SWCNTs in cells treated with nocodazole for G_2/M arrest indicates that NT uptake is heavily a premitotic phase event.

Simultaneously, the increase in endocytosis in early G_1 and reduction during late G_1/S suggest that a
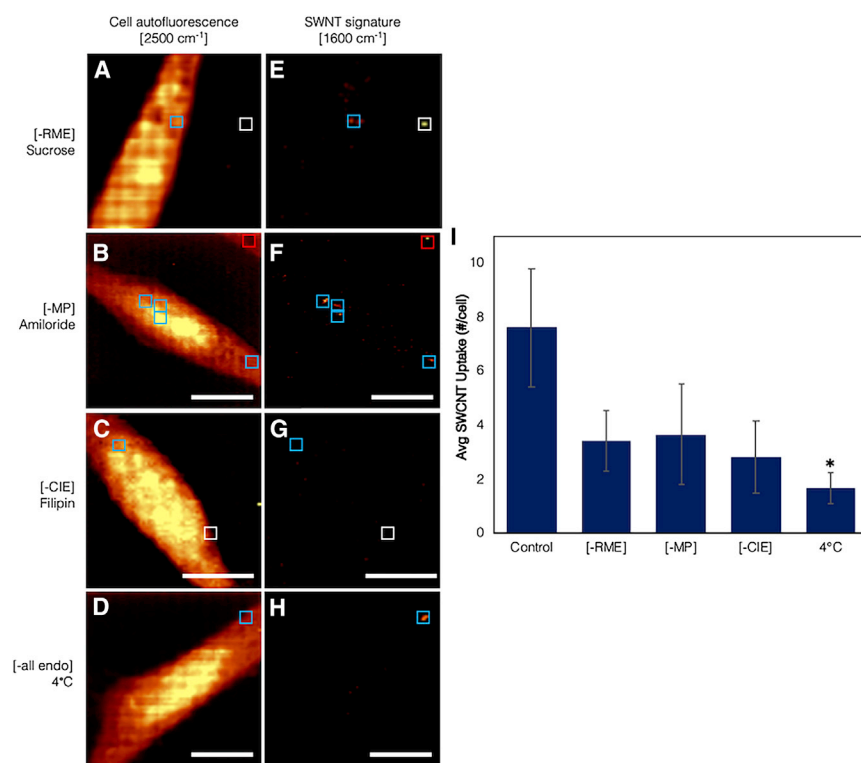
FIGURE 3 "Leave-one-out" testing of endocytic inhibition on uptake of DNA-SWCNTs in NSCs. Hyperspectral confocal imaging via Raman spectroscopy of (A–D) autofluorescence of NSCs and (E–H) DNA-SWCNTs in NSCs post endocytic inhibition of (A, E) RME via hypertonic sucrose, (B, F) macropinocytosis via amiloride, (C, G) clathrin-independent endocytosis via filipin, and (D, H) inhibition of all energy-dependent uptake at $4°C$ as compared with the asynchronous control seen in Fig. 2, D–H. SWCNTs with intracellular residency (*blue boxes*) confirmed by $100\times$ images taken at various points along the depth of the cell. Some SWCNTs remain adhered to the outer cell membrane (*white boxes*). Red boxes indicate bubbles and cosmic rays. (*I*) Average SWCNT uptake post endocytic inhibition treatments. *$p < 0.05$. Scale bars, 10 μm.

percentage of uptake happens in each phase and there is heterogeneity in mechanism of SWCNT uptake that is heavily cell cycle dependent. This aligns with the recent work done by the Gopal et al. on another material, which showed that the uptake of silicon nanoneedles was regulated by caveolae-mediated endocytosis and CME as well as MP simultaneously (48). Liu et al. detailed that carbon nanodiamonds, yet another material, sought entry into A549 human lung cancer epithelial cells via both MP and clathrin-dependent endocytosis (2). They noted nanodiamond presence in all phases of the cell cycle, including all phases of mitosis, causing no alteration of the spindle fibers nor chromosome segregation.

This, however, does not point to CME as solely responsible for the uptake of SWCNTs. Heterogeneity of clathrin-dependent uptake is based on variation in plasma membrane tension, which can depend highly on the state of the cell. Membrane tension is inversely related to the success of endocytosis. The stiffer the membrane, the less likely that endocytic machinery can generate forces to overcome that tension to bring materials into the cell. Membrane tension is also related to cell adhesion. When cell adhesion decreases, as in the case of cells preparing for mitosis, membrane tension is at its highest, indicating that CME should not be able to operate to traffic materials into the cell at the G_2/M phase in the cell cycle. The G_1, S, and G_2 phases themselves have shown nonhomogeneous adhesion of

the cell membrane (57). This presents a strong suggestion that although we have seen (19), and will continue to see below, that RME plays a role in the uptake of SWCNTs, there is strong heterogeneity of the contribution of diverse mechanisms of uptake that is heavily dependent on the cell membrane and cell-cycle dynamics.

It is important to note the role of the size of the cell on uptake. The surface area of the cell is known to vary highly with the progression of the cell cycle, often one of the determinant factors in advancement to the next phase of the cycle. Therefore, it is a realistic concern that a change in surface area of the cell could proportionately affect uptake during one phase as compared with another. To address this concern, the distribution of SWCNT uptake per cell per treatment and the corresponding cross-sectional surface area of each of those cells are shown in Fig. S2. Some treatments show a normal distribution of SWCNT uptake, where the mode of the data set corresponds to the mean/average presented in Fig. 2. There are a few outliers in the case of lovastatin and thymidine, for example, where we see the mode of the uptake data set is lower compared with the mean, yet this reduction is roughly consistent across all synchrony treatments. Along with low-value correlation coefficients, the data show a lack of correlation between the surface area of the cell and SWCNT uptake.

Finally, the percentage chance of a cell being asynchronous is roughly 10% for G_2/M, 27% for early G_1, and 15% for G_1/S. Therefore, of the cell scans collected, one, or at most two cell scans have a statistical chance of being an unsynchronized cell. This was counteracted by analyzing cells that showed a similar statistical distribution and assessing and excluding, if needed, the minimal number of outliers with significantly higher or lower NTs internalized. Ultimately, the synchronization was performed to maximally increase the yield of single-phase cells and increase the confidence in uptake numbers for each phase.

Inhibition of endocytic mechanisms for the study of DNA-SWCNT uptake pathways

To deepen the understanding of cell-cycle-based alteration of endocytic mechanisms and to test the contributions of specific methods of uptake for SWCNTs, "leave-one-out" endocytic inhibitory testing was conducted using: 1) hypertonic sucrose against RME; 2) amiloride against MP; and 3) filipin against CIE.

Each treatment knocked out one mechanism of endocytosis while leaving the remaining methods intact. Hypertonic sucrose causes clathrin to create microcages, rendering them inactive and bringing RME to a halt (58). Amiloride is an inhibitor of Na^+/H^+ exchangers, sodium channels, and Na^+/Ca^+ channels. For this reason it is used as an inhibitor of MP, although its exact mechanism of action is still unknown (59). Filipin binds to cholesterol in the membrane and prevents the invagination of calveolar pits, preventing calveolae-mediated endocytosis or CIE (60,61). Cells incubated with each of the endocytic inhibition treatments were assessed for the rates of viability to confirm the health of the cell populations. Table 1 shows high viabilities for each treatment, comparable with untreated, control NPCs. It is important to note that there is a lot of variability in endocytic inhibitors, and certain chemicals will often affect more than one method of endocytosis. Amiloride, for example, at certain concentrations, can arrest both MP and fast endophilin-mediated endocytosis (FEME) (62). This is an area of ongoing research, and many groups are simultaneously detangling new pathways, validating new cargoes, and deepening our understanding of conventional endocytic mechanisms and their inhibitors (24,25,63,64).

Fig. 3 shows the detailed data for post-endocytic inhibitory uptake of SWCNTs. Immediately evident is the reduction in uptake across the board from all treatments. The 55% reduction in endocytosis post inhibition of RME aligns with previous results and hypotheses, but 63% drop in SWCNT uptake in filipin-treated CIE-inhibited cells and 52% in MP-inhibited

cells implies that RME is aided in NT uptake by CIE and MP, as corroborated by studies previously cited on uptake of other nanomaterials in a range of cell types. These results reveal the equal participation of CIE and MP alongside RME in the internalization of SWCNTs. For complete inhibition, endocytosis was ceased by incubation at 4°C during NT uptake, knocking out all ATP-based endocytosis, including RME, MP, and CIE and leading to a 78% drop in uptake. This supports that the majority of DNA-SWCNT uptake in NPCs is energy dependent. While there is some evidence of energy-independent uptake via the lipid bilayer, studies by colleagues support the primary role of energy-dependent uptake of SWCNTs (47,65).The control remains the highest in uptake given that all methods of endocytosis, no matter whether primary or secondary, are accepting nanomaterials intracellularly.

Transferrin was used as a control and comparison for the above results, where its uptake is mediated by TfR only via RME. Transferrin is an iron-binding glycoprotein that facilitates the internalization of iron into the cell. It binds to iron tightly but reversibly and associates with the TfR membrane receptor to deliver iron intracellularly and be trafficked back out via recycling endosomes (66). If SWCNTs were internalized only by RME, a similar uptake trend would be seen for transferrin to match that of the SWCNTs, as both cargoes, though recognized by different receptors, would be internalized by the same CCVs. The comparison between transferrin and NTs is shown in Fig. 4. The largest drop in transferrin uptake is after inhibition of RME, as expected, and during early G_1. This reduction specifies that RME does not serve as a primary method of uptake during the earlier portion of the G_1 growth phase. Contrary to what was seen for NTs, transferrin internalization looks unchanged during late G_1/S. Transferrin uptake is shown in Fig. 4 *A* to actually increase when MP and CIE are inhibited, with an internalization higher than what is seen in the control cells, following the hypothesis that when one endocytic method is stunted, in this case RME, other methods will substitute. This phenomenon has been observed in other cargoes (63,67–69) prior to our findings.

The juxtaposition of the transferrin onto NT uptake proposes that, while RME is not the primary or sole mechanism responsible for SWCNT uptake during early G_1, the consistently higher internalization of transferrin during late G_1/S and G_2/M arrested cells shows that RME does have a role to play. Most interestingly, the data continue to indicate that there is likely multiple-mechanism co-uptake via each of the three endocytic pathways, leading to the drastic uptake of NTs during the G_2/M phase. The overall results strongly correlate with the hypothesis that nanomaterials gain
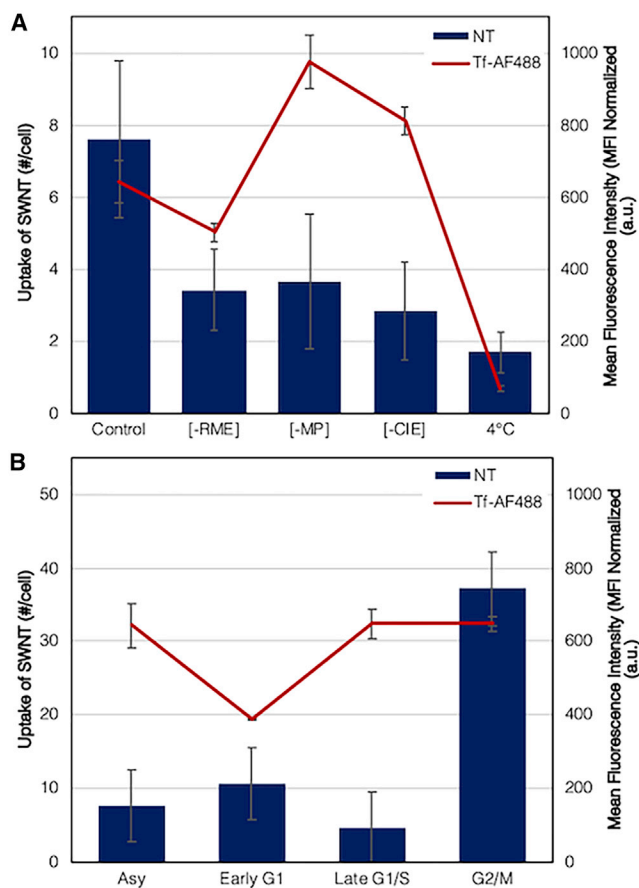
FIGURE 4 Uptake comparison of known RME-driven transferrin (Tf-AlexaFluor488) with SWCNTs during (*A*) synchrony and (*B*) endocytic inhibition. Transferrin uptake is lowest during RME and early G_1 phase of the cell cycle. Lack of consistency between NT and transferrin uptake shows that SWCNTs are perhaps internalized by multiple pathways of endocytosis.

entry into the cell by more than just one method, and that more than one method of endocytosis can be responsible for the uptake of a single cargo. The uptake of cargo (70,71) such as cholera toxin (72,73) and even nanomaterials (2,48,74) by multiple endocytic pathways have been recorded, and this field requires further investigation to understand the dynamics of nanomaterials, endocytic co-transport, and substitution during each phase of the cell cycle.

A potential contributing factor to multiple pathway uptake is the diversity in length of the SWCNTs introduced to the NSCs. This diversity comes from prolonged sonication utilized for single-NT dispersion—it is known to cause breakage at defective sites along the nanomaterial, leading to a diverse range of the lengths from 100 to 500 nm. Shortening of NTs caused by additional sonication of solution is a ubiquitously accepted side effect first mentioned by Shelimov et al. (75). Size dependency of endocytic uptake is a well-studied but case-based phenomenon that is also affected by shape and functionalization of the material. For DNA-SWCNTs specifically, evidence shows that uptake of cylindrical NTs was higher in rate than spherical gold nanoparticles, and that SWCNTs less than 100 nm in length have been shown to be taken up via RME (76). Some of the size ranges for canonical endocytosis methods based on a recent review (64) are approximately 100 nm in diameter for CME and clathrin-independent carrier/glycosylphosphatidylinositol-anchored protein enriched early endocytic compartment endocytosis. Sizes are thought to be 60 nm in diameter for caveolin-dependent endocytosis and roughly 60–80 nm in cylindrical diameter for FEME, but up to hundreds of nanometers in length. MP and phagocytosis lie at a particle acceptance size of >200 nm. Therefore, the range of lengths in the NTs used in this study is likely to instigate a range of endocytic mechanisms that would require further experimentation to unravel them.

Moving forward, there are also several important questions surrounding post-entry movement and trafficking of nanomaterials through the cell via RME, MP, and CIE individually to be studied. An interaction mapping from entry to exit of the SWCNTs in NPCs with focus on intracellular component reorganization and an examination of expression levels of the key proteins involved will build a better picture of endocytosis as it relates to cell-cycle regulation and cellular fate processes. Evidence that endocytosis is cell cycle dependent garners interest to revisit the phenomenon that the intracellular presence of the NTs has been shown to trigger an increase in the rate of differentiation of C17.2 NPCs (19,77). Cellular fate processes are well intertwined such that changes in one process triggers a cascade of downstream changes in associated processes. The endocytosis of nanomaterials triggers the typical endocytic pathway, but the size, shape, and functionalization alters the normal cascade in such a way that this path is thought to lead downstream to neural differentiation.

Conversely, at the disproportionate high dose of NTs administered for targeted gene- or drug-delivery applications without appropriate stable biofunctionalization, in some works evidence of cytotoxicity and reorganization of, or NT interaction with, intracellular components in various cell types has been reported (3,17,47,76,78–83). Many, in turn, argue against claims of cytotoxicity, stating that the specific type of nanomaterial, type of functionalization, and final working concentrations of the material will dramatically influence the degree of biocompatibility and are critical to take into account (7,13). Therefore, a deeper investigation of the influence of NTs on various cell types is required to debunk the controversial issue of the biocompatibility of nanomaterials and to better understand the mechanisms by

which intracellular interactions with well-defined nano-materials unfold.

Examining cell mechanics and biochemistry of a dynamic and adapting cell will strengthen the understanding of nanomaterial cell downstream interactions, including the positive and/or negative effects that NTs and nanomaterial-based therapeutics fundamentally have on neuronal cell populations and patients treated using these methods.

CONCLUSIONS

The progress in SWCNT and NPC interactions over this study uncovered the roles of RME, MP, and CIE as mechanisms of SWCNT uptake into NPCs. It unraveled the dependency of endocytosis mechanism on cell-cycle regulation in SWCNT uptake, where all three methods of endocytosis (RME, MP, and CIE) were shown to play differing phase-dependent roles that are thought to change based on variations in lipid bilayer membrane tension. Ultimately, uptake of SWCNTs was shown to drastically increase in premitotic G_2/M phase arrested cells and to decrease in G_1/S transition arrested cells.

A clearer picture of the relationship between endocytosis, cell cycle, and differentiation will be evident through the propagation of this field of work. For ailments such as Alzheimer's disease and Parkinson's disease, natural augmentation of neuronal differentiation as a supplement for poor neurogenesis (84) can ease symptoms and be the basis for a more permanent and safe treatment option. Although therapeutics are an extended goal, the mechanistic understanding of neural development can inspire the development of biosensors. Finally, a deeper understanding of the mechanisms by which SWCNTs alter NSCs both in positive and negative respects will give fuel to determining therapeutics capable of ensuring cell health and renewal against neurodegeneration.

SUPPORTING MATERIAL

Supporting material can be found online at https://doi.org/10.1016/j.bpr.2022.100061.

AUTHOR CONTRIBUTIONS

S.C. and S.S.J. designed the research. S.C., S.K., and A.I.V. performed the research. S.C. analyzed the data and wrote the paper. T.I. and S.V.R. provided guidance and valuable insights.

ACKNOWLEDGMENTS

DECLARATION OF INTERESTS

The authors declare no competing interests.

REFERENCES

1. Whitesides, G. M. 2003. The "right" size in nanobiotechnology. *Nat. Biotechnol.* 21:1161–1165. https://doi.org/10.1038/nbt872.

2. Liu, K. K., C. C. Wang, …, J. I. Chao. 2009. Endocytic carboxylated nanodiamond for the labeling and tracking of cell division and differentiation in cancer and stem cells. *Biomaterials.* 30:4249–4259. https://doi.org/10.1016/j.biomaterials.2009.04.056.

3. Holt, B. D., H. Shams, …, K. N. Dahl. 2012. Altered Cell Mechanics from the Inside: Dispersed Single Wall Carbon Nanotubes Integrate with and Restructure Actin. *J. Funct. Biomater.* 3:398–417. https://doi.org/10.3390/jfb3020398.

4. Mundra, R. V., X. Wu, …, R. S. Kane. 2014. Nanotubes in biological applications. *Curr. Opin. Biotechnol.* 28:25–32. https://doi.org/10.1016/j.copbio.2013.10.012.

5. Hong, G., S. Diao, …, H. Dai. 2015. Carbon Nanomaterials for Biological Imaging and Nanomedicinal Therapy. *Chem. Rev.* 115:10816–10906. https://doi.org/10.1021/acs.chemrev.5b00008.

6. Merum, S., J. B. Veluru, and R. Seeram. 2017. Functionalized carbon nanotubes in bio-world: Applications, limitations and future directions. *Mater Sci. Eng. B.* 223:43–63. https://doi.org/10.1016/j.mseb.2017.06.002.

7. Madani, S. Y., A. Mandel, and A. M. Seifalian. 2013. A concise review of carbon nanotube's toxicology. *Nano Rev.* 4:21521. https://doi.org/10.3402/nano.v4i0.21521.

8. Asghar, W., H. Shafiee, …, U. Demirci. 2016. Toxicology study of single-walled carbon nanotubes and reduced graphene oxide in human sperm. *Sci. Rep.* 6:30270. https://doi.org/10.1038/srep30270.

9. Fadeel, B., and K. Kostarelos. 2020. Grouping all carbon nanotubes into a single substance category is scientifically unjustified. *Nat. Nanotechnol.* 15:164. https://doi.org/10.1038/s41565-020-0654-0.

10. Zheng, M., A. Jagota, …, N. G. Tassi. 2003. DNA-assisted dispersion and separation of carbon nanotubes. *Nat. Mater.* 2:338–342. https://doi.org/10.1038/nmat877.

11. Strano, M. S., M. Zheng, …, M. L. Usrey. 2004. Understanding the nature of the DNA-assisted separation of single-walled carbon nanotubes using fluorescence and Raman spectroscopy. *Nano Lett.* 4:543–550. https://doi.org/10.1021/nl034937k.

12. Zheng, M., A. Jagota, …, D. J. Walls. 2003. Structure-Based Carbon Nanotube Sorting by Sequence-Dependent DNA Assembly. *Science.* 302:1545–1548. https://doi.org/10.1126/science.1091911.

13. Krug, H. F. 2014. Nanosafety research-are we on the right track? *Angew. Chem. Int. Ed.* 53:12304–12319. https://doi.org/10.1002/anie.201403367.

14. Xue, X., L. R. Wang, …, X. J. Liang. 2014. Single-walled carbon nanotubes alleviate autophagic/lysosomal defects in primary glia from a mouse model of alzheimers disease. *Nano Lett.* 14:5110–5117. https://doi.org/10.1021/nl501839q.

15. Xue, X., J.-Y. Yang, …, X. J. Liang. 2016. Aggregated single-walled carbon nanotubes attenuate the behavioural and neurochemical effects of methamphetamine in mice. *Nat. Nanotechnol.* 11:613. https://doi.org/10.1038/nnano.2016.23.

16. Lee, H. J., J. Park, …, S. S. Kim. 2011. Amine-modified single-walled carbon nanotubes protect neurons from injury in a rat

stroke model. *Nat. Nanotechnol.* 6:121–125. https://doi.org/10.1038/nnano.2010.281.

17. Ignatova, T., S. Chandrasekar, …, S. V. Rotkin. 2017. Micro-Raman spectroscopy as an enabling tool for long-term intracellular studies of nanomaterials at nanomolar concentration levels. *J. Mater. Chem. B.* 5:6536–6545. https://doi.org/10.1039/c7tb00766c.

18. Horoszko, C. P., P. V. Jena, …, D. A. Heller. 2019. Optical Voltammetry of Polymer-Encapsulated Single-Walled Carbon Nanotubes. *J. Phys. Chem. C.* 123:24200–24208. https://doi.org/10.1021/acs.jpcc.9b07626.

19. Pirbhai, M., S. Chandrasekar, …, S. S. Jedlicka. 2019. Augmentation of C17.2 Neural Stem Cell Differentiation via Uptake of Low Concentrations of ssDNA-Wrapped Single-Walled Carbon Nanotubes. *Adv. Biosyst.* 3:1800321. https://doi.org/10.1002/adbi.201800321.

20. Ferreira, L., J. M. Karp, …, R. Langer. 2008. New Opportunities: The Use of Nanotechnologies to Manipulate and Track Stem Cells. *Cell Stem Cell.* 3:136–146. https://doi.org/10.1016/j.stem.2008.07.020.

21. Stephanopoulos, N., R. Freeman, …, S. I. Stupp. 2015. Bioactive DNA-peptide nanotubes enhance the differentiation of neural stem cells into neurons. *Nano Lett.* 15:603–609. https://doi.org/10.1021/nl504079q.

22. Chen, C.-S., S. Soni, …, W. C. Chin. 2012. Human stem cell neuronal differentiation on silk-carbon nanotube composite. *Nanoscale Res. Lett.* 7:1–7. https://doi.org/10.1186/1556-276X-7-126.

23. Scapin, G., T. Bertalot, …, F. Filippini. 2016. Neuronal commitment of human circulating multipotent cells by carbon nanotube-polymer scaffolds and biomimetic peptides. *Nanomedicine.* 11:1929–1946. https://doi.org/10.2217/nnm-2016-0150.

24. Casamento, A., and E. Boucrot. 2020. Molecular mechanism of Fast Endophilin-Mediated Endocytosis. *Biochem. J.* 477:2327–2345. https://doi.org/10.1042/BCJ20190342.

25. Renard, H. F., and E. Boucrot. 2021. Unconventional endocytic mechanisms. *Curr. Opin. Cell Biol.* 71:120–129. https://doi.org/10.1016/j.ceb.2021.03.001.

26. Holtzer, H., H. Weintraub, …, B. Mochan. 1972. The cell cycle, cell lineages, and cell differentiation. *Curr. Top. Dev. Biol.* 7:229–256. https://doi.org/10.1016/S0070-2153(08)60073-3.

27. Hartwell, L. H., and T. A. Weinert. 1989. Checkpoints: controls that ensure the order of cell cycle events. *Science.* 246:629–634. https://doi.org/10.1126/science.2683079.

28. Fürthauer, M., and M. González-Gaitán. 2009. Endocytosis and mitosis: A two-way relationship. *Cell Cycle.* 8:3311–3318. https://doi.org/10.4161/cc.8.20.9700.

29. Scita, G., and P. P. Di Fiore. 2010. The endocytic matrix. *Nature.* 463:464–473. https://doi.org/10.1038/nature08910.

30. Fielding, A. B., A. K. Willox, …, S. J. Royle. 2012. Clathrin-mediated endocytosis is inhibited during mitosis. *Proc. Natl. Acad. Sci. U S A.* 109:6572–6577. https://doi.org/10.1073/pnas.1117401109.

31. Tacheva-Grigorova, S. K., A. J. M. Santos, …, T. Kirchhausen. 2013. Clathrin-mediated endocytosis persists during unperturbed mitosis. *Cell Rep.* 4:659–668. https://doi.org/10.1016/j.celrep.2013.07.017.

32. Mettlen, M., P.-H. Chen, …, S. L. Schmid. 2018. Regulation of Clathrin-Mediated Endocytosis. *Annu. Rev. Biochem.* 87. https://doi.org/10.1146/annurev-biochem-062917-012644.

33. Hinze, C., and E. Boucrot. 2018. Endocytosis in proliferating, quiescent and terminally differentiated cells. *J. Cell Sci.* 131:jcs216804. https://doi.org/10.1242/jcs.216804.

34. Kim, J. A., C. Aberg, …, K. A. Dawson. 2012. Role of cell cycle on the cellular uptake and dilution of nanoparticles in a cell population. *Nat. Nanotechnol.* 7:62–68. https://doi.org/10.1038/nnano.2011.191.

35. Snyder, E. Y., D. L. Deitcher, …, C. L. Cepko. 1992. Multipotent neural cell lines can engraft and participate in development of mouse cerebellum. *Cell.* 68:33–51. https://doi.org/10.1016/0092-8674(92)90204-P.

36. Rosner, M., K. Schipany, and M. Hengstschläger. 2013. Merging high-quality biochemical fractionation with a refined flow cytometry approach to monitor nucleocytoplasmic protein expression throughout the unperturbed mammalian cell cycle. *Nat. Protoc.* 8:602–626. https://doi.org/10.1038/nprot.2013.011.

37. Zhang, E., X. Li, …, X. Zheng. 2005. Cell cycle synchronization of embryonic stem cells: Effect of serum deprivation on the differentiation of embryonic bodies in vitro. *Biochem. Biophys. Res. Commun.* 333:1171–1177. https://doi.org/10.1016/j.bbrc.2005.05.200.

38. Tate, S., and P. Ko Ferrigno. 2006. Cell cycle: synchronization at various stages. *Encycl. Life Sci.* 1:1–5. https://doi.org/10.1038/npg.els.0002570.

39. Kallas, A., M. Pook, …, T. Maimets. 2011. Nocodazole treatment decreases expression of pluripotency markers nanog and Oct4 in human embryonic stem cells. *PLoS One.* 6. https://doi.org/10.1371/journal.pone.0019114.

40. Pauklin, S., and L. Vallier. 2013. The cell-cycle state of stem cells determines cell fate propensity. *Cell.* 155:135. https://doi.org/10.1016/j.cell.2013.08.031.

41. Keyomarsi, K., L. Sandoval, …, A. B. Pardee. 1991. Synchronization of tumor and normal cells from G1 to multiple cell cycles by lovastatin. *Cancer Res.* 51:3602–3609.

42. Dowdy, S., P. K. Davis, …, S. F. Dowdy. 2014. Biological methods for cell-cycle synchronization of mammalian cells. *Biotechniques.* 30:1322–1331. https://doi.org/10.2144/01306rv01.

43. Martínez-Botas, J., A. J. Ferruelo, …, M. A. Lasunción. 2001. Dose-dependent effects of lovastatin on cell cycle progression. Distinct requirement of cholesterol and non-sterol mevalonate derivatives. *Biochim. Biophys. Acta.* 1532:185–194. https://doi.org/10.1016/S1388-1981(01)00125-1.

44. Jakóbisiak, M., S. Bruno, …, Z. Darzynkiewicz. 1991. Cell cycle-specific effects of lovastatin. *Proc. Natl. Acad. Sci. U S A.* 88:3628–3632. https://doi.org/10.1073/pnas.88.9.3628.

45. Vasquez, R. J., B. Howell, …, L. Cassimeris. 1997. Nanomolar concentrations of nocodazole alter microtubule dynamic instability in vivo and in vitro. *Mol. Biol. Cell.* 8:973–985. https://doi.org/10.1091/mbc.8.6.973.

46. Cooper, S. 2003. Rethinking synchronization of mammalian cells for cell cycle analysis. *Cell. Mol. Life Sci.* 60:1099–1106. https://doi.org/10.1007/s00018-003-2253-2.

47. Bhattacharya, S., D. Roxbury, …, A. Jagota. 2013. DNA conjugated SWCNTs enter endothelial cells via Rac1 mediated macropinocytosis. *Nano Lett.* 12:1826–1830. https://doi.org/10.1021/nl204058u.

48. Gopal, S., C. Chiappini, …, M. M. Stevens. 2019. Porous silicon nanoneedles modulate endocytosis to deliver biological payloads. *Adv. Mater.* 31:1806788. https://doi.org/10.1002/adma.201806788.

49. Fittipaldi, A., A. Ferrari, …, M. Giacca. 2003. Cell membrane lipid rafts mediate caveolar endocytosis of HIV-1 tat fusion proteins. *J. Biol. Chem.* 278:34141–34149. https://doi.org/10.1074/jbc.M303045200.

50. Richard, J. P., K. Melikov, …, L. V. Chernomordik. 2005. Cellular uptake of unconjugated TAT peptide involves clathrin-dependent endocytosis and heparan sulfate receptors. *J. Biol. Chem.* 280:15300–15306. https://doi.org/10.1074/jbc.M401604200.

51. Kang, J. W., F. T. Nguyen, …, D. A. Heller. 2012. Measuring uptake dynamics of multiple identifiable carbon nanotube species via high-speed confocal Raman imaging of live cells. *Nano Lett.* https://doi.org/10.1021/nl302991y.

52. Romero, G., E. Rojas, …, S. E. Moya. 2011. Spontaneous confocal Raman microscopy-a tool to study the uptake of nanoparticles

and carbon nanotubes into cells. *Nanoscale Res. Lett.* 6:429. https://doi.org/10.1186/1556-276X-6-429.

53. Estrela-Lopis, I., G. Romero, …, E. Donath. 2011. Nanoparticle uptake and their co-localization with cell compartments - A confocal Raman microscopy study at single cell level. *J. Phys. Conf. Ser.* 304:012017. https://doi.org/10.1088/1742-6596/304/1/012017.

54. Yehia, H. N., R. K. Draper, …, P. Pantano. 2007. Single-walled carbon nanotube interactions with HeLa cells. *J. Nanobiotechnol.* 5:8. https://doi.org/10.1186/1477-3155-5-8.

55. Santos, A. J. M., and E. Boucrot. 2018. Chapter 3: Probing endocytosis during the cell cycle with minimal experimental perturbation. *Methods Mol. Biol.* 1847:749–754.

56. Royle, S. J., N. A. Bright, and L. Lagnado. 2005. Clathrin is required for the function of the mitotic spindle. *Nature.* 434:1152–1157. https://doi.org/10.1038/nature03502.

57. Djakbarova, U., Y. Madraki, …, C. Kural. 2021. Dynamic interplay between cell membrane tension and clathrin-mediated endocytosis. *Biol. Cell.* 113:344–373. https://doi.org/10.1111/boc.202000110.

58. Dutta, D., and J. G. Donaldson. 2012. Search for inhibitors of endocytosis: Intended specificity and unintended consequences. *Cell. Logist.* 2:203–208. https://doi.org/10.4161/cl.23967.

59. Koivusalo, M., C. Welch, …, S. Grinstein. 2010. Amiloride inhibits macropinocytosis by lowering submembranous pH and preventing Rac1 and Cdc42 signaling. *J. Cell Biol.* 188:547–563. https://doi.org/10.1083/jcb.200908086.

60. Orlandi, P. A., and P. H. Fishman. 1998. Filipin-dependent inhibition of cholera toxin: Evidence for toxin internalization and activation through caveolae-like domains. *J. Cell Biol.* 141:905–915. https://doi.org/10.1083/jcb.141.4.905.

61. Torgersen, M. L., G. Skretting, …, K. Sandvig. 2001. Internalization of cholera toxin by different endocytic mechanisms. *J. Cell Sci.* 114:3737–3747.

62. Boucrot, E., A. P. A. Ferreira, …, H. T. McMahon. 2015. Endophilin marks and controls a clathrin-independent endocytic pathway. *Nature.* 517:460–465. https://doi.org/10.1038/nature14067.

63. Ferreira, A. P. A., and E. Boucrot. 2018. Mechanisms of carrier formation during clathrin-independent endocytosis. *Trends Cell Biol.* 28:188–200. https://doi.org/10.1016/j.tcb.2017.11.004.

64. Rennick, J. J., A. P. R. Johnston, and R. G. Parton. 2021. Key principles and methods for studying the endocytosis of biological and nanoparticle therapeutics. *Nat. Nanotechnol.* 16:266–276. https://doi.org/10.1038/s41565-021-00858-8.

65. Yaron, P. N., B. D. Holt, …, K. N. Dahl. 2011. Single wall carbon nanotubes enter cells by endocytosis and not membrane penetration. *J. Nanobiotechnol.* 9:1–15.

66. Mayle, K. M., A. M. Le, and D. T. Kamei. 2012. The intracellular trafficking pathway of transferrin. *Biochim. Biophys. Acta.* 1820:264–281. https://doi.org/10.1016/j.bbagen.2011.09.009.

67. Boucrot, E., S. Saffarian, …, T. Kirchhausen. 2010. Roles of AP-2 in clathrin-mediated endocytosis. *PLoS One.* 5. https://doi.org/10.1371/journal.pone.0010597.

68. Utskarpen, A., R. Massol, …, K. Sandvig. 2010. Shiga toxin increases formation of clathrin-coated pits through syk kinase. *PLoS One.* 5:e10944. https://doi.org/10.1371/journal.pone.0010944.

69. Massol, R. H., J. E. Larsen, …, T. Kirchhausen. 2004. Cholera toxin toxicity does not require functional Arf6- and dynamin-dependent endocytic pathways. *Mol. Biol. Cell.* 15:3631–3641. https://doi.org/10.1091/mbc.e04-04-0283.

70. Malyukova, I., K. F. Murray, …, O. Kovbasnjuk. 2009. Macropinocytosis in Shiga toxin 1 uptake by human intestinal epithelial cells and transcellular transcytosis. *Am. J. Physiol. Gastrointest. Liver Physiol.* 296:78–92. https://doi.org/10.1152/ajpgi.90347.2008.

71. Lei, J. T., and M. Martinez-Moczygemba. 2008. Separate endocytic pathways regulate IL-5 receptor internalization and signaling. *J. Leukoc. Biol.* 84:499–509. https://doi.org/10.1189/jlb.1207828.

72. Chalovich, J. M., and E. Eisenberg. 2005. Rafting with cholera toxin. *Biophys. Chem.* 257:2432–2437. https://doi.org/10.1111/j.1574-6968.2006.00545.x.

73. Hansen, G. H., S. M. Dalskov, …, E. M. Danielsen. 2005. Cholera toxin entry into pig enterocytes occurs via a lipid raft- and clathrin-dependent mechanism. *Biochemistry.* 44:873–882. https://doi.org/10.1021/bi047959+.

74. Sahay, G., D. Y. Alakhova, and A. V. Kabanov. 2010. Endocytosis of nanomedicines. *J. Control. Release.* 145:182–195. https://doi.org/10.1016/j.jconrel.2010.01.036.

75. Shelimov, K. B., R. O. Esenaliev, …, R. E. Smalley. 1998. Purification of single-wall carbon nanotubes by ultrasonically assisted filtration. *Chem. Phys. Lett.* 282:429–434. https://doi.org/10.1016/S0009-2614(97)01265-7.

76. Jin, H., D. A. Heller, …, M. S. Strano. 2009. Size-dependent cellular uptake and expulsion of single-walled carbon nanotubes: single particle tracking and a generic uptake model for nanoparticles. *ACS Nano.* 3:149–158. https://doi.org/10.1021/nn800532m.

77. Pirbhai, M. 2015. Influence of bio-functionalized single walled carbon nanotubes on neural stem cells. *In* ProQuest Dissertation & Theses, p. 148. http://search.proquest.com/docview/1722047843?accountid=14701%5Cnhttp://sfx.scholarsportal.info/ottawa?url_ver=Z39.88-2004&rft_val_fmt=info:ofi/fmt:kev:mtx:dissertation&genre=dissertations+%26+theses&sid=ProQ:ProQuest+Dissertations+%26+Theses+Global&atitl.

78. Jin, H., D. A. Heller, and M. S. Strano. 2008. Single-particle tracking of endocytosis and exocytosis of single-walled carbon nanotubes in NIH-3T3 Cells 2008. *Nano Lett.* 8:1577–1585.

79. Holt, B. D., K. N. Dahl, and M. F. Islam. 2011. Quantification of uptake and localization of bovine serum albumin-stabilized single-wall carbon nanotubes in different human cell types. *Small.* 7:2348–2355. https://doi.org/10.1002/smll.201100437.

80. Shams, H., B. D. Holt, …, M. R. K. Mofrad. 2014. Actin reorganization through dynamic interactions with single-wall carbon nanotubes. *ACS Nano.* 8:188–197. https://doi.org/10.1021/nn402865e.

81. Alidori, S., R. L. Bowman, …, D. L. Thorek. 2016. Deconvoluting hepatic processing of carbon nanotubes. *Nat. Commun.* 1–11. https://doi.org/10.1038/ncomms12343.

82. Hansel, C. S., S. W. Crowder, …, M. M. Stevens. 2019. Nanoneedle-mediated stimulation of cell mechanotransduction machinery. *ACS Nano.* 13:2913–2926. https://doi.org/10.1021/acsnano.8b06998.

83. Belyanskaya, L., S. Weigel, …, P. Wick. 2009. Effects of carbon nanotubes on primary neurons and glial cells. *Neurotoxicology.* 30:702–711. https://doi.org/10.1016/j.neuro.2009.05.005.

84. Moreno-Jiménez, E. P., M. Flor-García, …, M. Llorens-Martín. 2019. Adult hippocampal neurogenesis is abundant in neurologically healthy subjects and drops sharply in patients with Alzheimer's disease. *Nat. Med.* 25:554–560. https://doi.org/10.1038/s41591-019-0375-9.